Journal of CO_2 Utilization 17 (2017) 220–234

Contents lists available at ScienceDirect

Journal of CO_2 Utilization

journal homepage: www.elsevier.com/locate/jcou

CO_2 conversion in a gliding arc plasma: Performance improvement based on chemical reaction modeling

S.R. Sun[a,b], H.X. Wang[a,*], D.H. Mei[c], X. Tu[c], A. Bogaerts[b,*]

[a] School of Astronautics, Beihang University, 100191, Beijing, China
[b] Research Group PLASMANT, Department of Chemistry, University of Antwerp, Universiteitsplein 1, B-2610 Antwerp, Belgium
[c] Department of Electrical Engineering and Electronics, University of Liverpool, Liverpool L69 3GJ, United Kingdom

ARTICLE INFO

Article history:
Received 14 November 2016
Received in revised form 10 December 2016
Accepted 20 December 2016
Available online xxx

Keywords:
CO_2 conversion
Gliding arc
Energy efficiency

ABSTRACT

CO_2 conversion into value-added chemicals is gaining increasing interest in recent years, and a gliding arc plasma has great potential for this purpose, because of its high energy efficiency. In this study, a chemical reaction kinetics model is presented to study the CO_2 splitting in a gliding arc discharge. The calculated conversion and energy efficiency are in good agreement with experimental data in a range of different operating conditions. Therefore, this reaction kinetics model can be used to elucidate the dominant chemical reactions contributing to CO_2 destruction and formation. Based on this reaction pathway analysis, the restricting factors for CO_2 conversion are figured out, i.e., the reverse reactions and the small treated gas fraction. This allows us to propose some solutions in order to improve the CO_2 conversion, such as decreasing the gas temperature, by using a high frequency discharge, or increasing the power density, by using a micro-scale gliding arc reactor, or by removing the reverse reactions, which could be realized in practice by adding possible scavengers for O atoms, such as CH_4. Finally, we compare our results with other types of plasmas in terms of conversion and energy efficiency, and the results illustrate that gliding arc discharges are indeed quite promising for CO_2 conversion, certainly when keeping in mind the possible solutions for further performance improvement.

1. Introduction

CO_2 is a major greenhouse gas contributing to global warming [1]. Hence, in recent years the conversion of CO_2 into value-added chemicals or new fuels is gaining much interest, using a variety of conversion methods [2–9]. A novel methodology that shows great promise is based on plasma technology [10]. Plasma is an ionized gas, which is typically created by applying electric power to a gas. It is a highly reactive chemical cocktail, consisting of neutral gas molecules, but also various radicals, atoms, ions and electrons. We can make a distinction between thermal and non-thermal plasmas. In a thermal plasma, all species have the same energy and are in so-called thermal equilibrium with each other. In a non-thermal plasma, the electrons have much higher energy than the other plasma species. Indeed, the applied electric power mostly heats the electrons, due to their small mass, and they can activate the gas molecules by electron impact excitation, ionization and dissociation collisions. Hence, the gas itself does not have to be heated in order to be activated. In this way, thermodynamically unfavorable reactions, like CO_2 conversion, can proceed with reasonable energy cost, at mild operating conditions (ambient pressure and temperature). Besides thermal and non-thermal plasmas, there is also an intermediate group of so-called warm plasmas, with somewhat higher gas temperature, and an electron temperature that is somewhat lower than in typical non-thermal plasmas. Indeed, in non-thermal plasmas the electrons typically have energy of about 2–3 eV, while in warm plasmas they typically have energy of about 1 eV. The latter is more suitable for vibrational excitation of CO_2 molecules, which is known to be the most energy efficient pathway for CO_2 dissociation [10]. This selective excitation to the vibrational modes, but also the selective excitation of other degrees of freedom, forms the basis of the non-equilibrium character of plasma, which will enhance the chemical selectivity. As mentioned above, in the context of CO_2 conversion, especially the selective electron impact excitation to the vibrational levels can optimize the energy efficiency. Indeed, it requires only a limited amount of electron energy to populate the lowest vibrational levels of CO_2, and subsequently, the vibrational levels exchange energy among each other, gradually populating the

* Corresponding authors.
E-mail addresses: whx@buaa.edu.cn (H.X. Wang), annemie.bogaerts@uantwerpen.be (A. Bogaerts).

http://dx.doi.org/10.1016/j.jcou.2016.12.009
2212-9820/

higher levels (i.e., so-called vibrational-vibration relaxation or ladder climbing), up to the dissociation limit. In this way, only limited amount of energy must be spent for dissociation of the CO_2 molecules. This is in contrast to the situation where CO_2 dissociation occurs upon electron impact electronic excitation, as is the case in non-thermal plasmas, where the electrons have somewhat higher energy. Indeed, it requires about 7–10 eV to electronically excite the CO_2 molecules to a dissociative level. This energy is much more than the OC=O bond energy (5.5 eV), which means that some electron energy is just lost, i.e., waste of energy. The selective excitation of the CO_2 vibrational levels is thus crucial to maximize the energy efficiency. In the 1970s and 1980s, CO_2 dissociation by various types of non-equilibrium plasmas was already extensively studied both theoretically and experimentally, with emphasis on selective vibrational excitation [11–16]. More recently, the research on plasma-based CO_2 conversion gained renewed interest, and several groups were studying the performance of various types of plasma reactors, including dielectric barrier discharges (DBDs) [17–34], microwave plasmas [35–41], ns-pulsed [42] and spark discharges [43–47], as well as gliding arc (GA) discharges [48–60].

Computer modeling can be very useful in gaining a better understanding of the decomposition process of CO_2, since it can deal with a huge number of chemical reactions in plasma and it can clarify our understanding of the complex processes related to CO_2 decomposition. Moreover, computer simulations can provide data which are difficult to measure, such as the densities of individual vibrational levels, reaction rates, etc, and it also can help to identify the most important chemical reaction processes or parameters. Therefore, in order to improve the performance of various types of plasma reactors for CO_2 decomposition, computer modeling can be very useful, as it allows to obtain better insight in the underlying mechanisms. To date, a number of computer models have been developed for DBD and microwave plasma [17–19,23,39], but to our knowledge, no theoretical modeling on the conversion and energy efficiency of CO_2 in a GA discharge has been published yet, although this type of plasma is very promising in terms of conversion and energy efficiency, and many experiments have been performed to study pure CO_2 splitting [48–50] as well as the combined conversion of CO_2 with CH_4, i.e., dry reforming, to yield syngas and other useful products, such as methanol and formaldehyde [51–55].

A GA discharge is a non-stationary arc discharge between two diverging electrodes submerged in a gas flow. The arc is ignited at the shortest electrode distance and pushed by the gas flow towards the diverging electrode region. The arc length grows together with the voltage, when the arc length exceeds its critical value, a fast transition into a non-equilibrium regime occurs. Subsequently, the arc glides under non-equilibrium conditions [61–64]. Therefore, for most prospective plasma chemical applications, for example, the decomposition of CO_2, the GA discharges simultaneously has the advantages of high electron temperature and high electron density for high reactor productivity and a high degree of non-equilibrium to support selective chemical processes, like vibrational excitation (see above).

One of the main research efforts in plasma-based CO_2 splitting, not only in GA discharges but also in the other plasma reactors, is to maximize the conversion and energy efficiency. A GA plasma exhibits a rather high energy efficiency, i.e., for dry reforming of methane (DRM), a maximum energy efficiency of around 60% was achieved at an input power of 165 W and a feed gas flow rate of 7.5 L/min, at a conversion in the range of 8–16% [53]. For pure CO_2 splitting, a maximum conversion of 18% was obtained at a low gas flow rate of 0.8 L/min and a high discharge power of about 200 W [49], but the corresponding energy efficiency was only about 14%. For a vortex-flow GA, a maximum energy efficiency of 43% was reported for pure CO_2 splitting, at a high gas flow rate of 27 L/min, but the estimated conversion under this condition was only about 5% [48].

Usually, the increase of conversion upon increasing discharge power or decreasing gas flow rate is accompanied by a reduction in the energy efficiency, due to the higher values of the specific energy input (SEI), and vice versa, the energy efficiency is enhanced at high gas flow rate or lower discharge power, but at the expense of the conversion. Therefore, a number of experiments have been performed in literature, for example, by adding some auxiliary gases [49,56], by varying the GA discharge structure [57–59] or by combination with a catalyst [57,60], to pursue the most promising conversion and energy efficiency simultaneously in a GA plasma. The addition of N_2 as auxiliary gas on the CO_2 conversion has been investigated in [49], and the CO_2 conversion was reported to reach values up to 35% at a N_2 concentration of 95%, which is higher than the conversion of 15–18% reported for pure CO_2. At the same time, the power (or energy) efficiency was found to increase by about a factor three compared to pure CO_2. In [56] CH_4 was added as the auxiliary gas, yielding a maximum CO_2 conversion of 34.5%, which is again larger than the value obtained (12.3%) when only pure CO_2 was supplied, and showing an energy efficiency of about 70%. In addition, the reactor geometry can also have a significant effect on the conversion. For instance, a micro-scale GA reactor is characterized by a higher power density, and thus, in the case of CH_4 conversion, a higher conversion of 32% was observed [57], while in a conventional GA reactor, a lower conversion of 18% and 8% was obtained in pure CH_4 and in a CH_4/He mixture, respectively [55]. Besides a classical GA between two flat electrodes, a rotating GA plasma also exhibits good performance for both conversion and energy efficiency, due to the enlarged reaction region [58,59]. The conversion of CH_4 reaches 36%, corresponding to the energy efficiency of 26.7% for dry reforming of methane in a rotating GA discharge [58]. Finally, a combination of a GA discharge with catalysts is also promising to improve the conversion and energy efficiency, and furthermore, it has an important influence on the product selectivity. In [57], a CH_4 conversion of about 50% was achieved in a GA plasma with Ni-loaded catalyst. Moreover, the combination of a GA plasma with catalysts in a heat-insulated reactor has shown to yield a dramatic rise in energy efficiency (up to 86%) with a CH_4 conversion of 92% and a CO_2 conversion of 20% [60].

From these experimental results, it seems that GA discharges are indeed promising for CO_2 conversion. However, the chemical mechanisms of the conversion are still not fully understood. We believe that a thorough understanding of these chemical mechanisms is indispensable to further improve the performance of the GA plasma in terms of conversion and energy efficiency. This thorough understanding can be obtained by computer simulations. The latter will also allow us to elucidate the restricting factors in the conversion, which is needed to provide possible solutions on how to improve the conversion and energy efficiency, based on the CO_2 splitting chemical kinetics mechanisms.

Building a two-dimensional (2D) [65] or three-dimensional (3D) model [66] for CO_2 conversion in a GA discharge is an extremely challenging task in view of computation time, due to the complex CO_2 chemistry. Indeed, from our experience with modeling a DBD and MW plasma [17–19,39], we expect that besides ground state neutral species, also ions, electronically excited and especially vibrationally excited CO_2 molecules play a major role in the conversion process, so these species should be included in the model for a GA plasma as well. Therefore, we focus here on the detailed chemical reaction kinetics of CO_2 splitting in a GA discharge, including the vibrationally and electronically excited states, by means of a zero-dimensional (0D) chemical reaction kinetics model [67,68].

In order to apply a 0D model to the GA plasma conditions and geometry, we need to make several assumptions. The latter will be based on the specific experimental setup for which experimental data are obtained to validate our model, as presented in Section 2. Furthermore, we already have experience in building 2D and 3D models for argon in a GA [65,66], and the knowledge obtained from these models will be used as input in the present 0D model. A brief explanation about the 0D model, as well as the chemical reactions considered in the model are given in Section 3, while the detailed model assumptions for the GA discharge are discussed in Section 4. The modeling results will be presented in Section 5, including the comparison with experimental data to validate the model, and an analysis of the chemical reaction mechanisms. By means of the computer simulations, validated by experiments, we will be able to elucidate the main chemical reactions contributing to the CO_2 destruction and formation and to identify the restricting factors, which will allow us to suggest possible improvements in terms of CO_2 conversion and energy efficiency in a GA discharge. Finally, the conversion and energy efficiency obtained in this work will be compared with the best results reported in literature for a GA plasma, as well as for other plasma types, to place our results in a broader perspective on plasma-based CO_2 conversion.

2. Experimental setup of the GA reactor

A schematic diagram of the experimental GA reactor is shown in Fig. 1 [69,70]. A pair of semi-ellipsoidal electrodes (50 mm long, 30 mm wide and 5 mm thick) is fixed in an insulating bracket and symmetrically placed on both sides of a gas nozzle in a cylindrical container, with diameter of 160 mm and height of 191 mm. Both electrodes are connected to a neon transformer (SIET, 230 V/10 kV, 50 Hz). The discharge ignites at the shortest interelectrode distance, and subsequently the arc is pushed by the gas flow along the electrodes until it extinguishes when the distance between both electrodes becomes too large, after which a new arc is established at the shortest interelectrode distance. Thus, the arc cycle repeats itself. The shortest interelectrode distance can be varied from 1 mm to 5 mm, in order to change the amount of gas passing through the electrodes. In our experiments and simulations, an interelectrode distance of 2, 2.5 and 3 mm is considered. CO_2 (99.8%, BOC UK) gas is injected into the reactor through the gas nozzle at the bottom of the reactor, and the gas leaving the reactor at the outlet (see Fig. 1) is a mixture of CO_2, partially converted into CO and O_2. These gases are analyzed by a two-channel gas chromatograph (Shimadzu 2014), which is equipped with a flame ionization detector (FID) and a thermal conductivity detector (TCD). The CO_2 conversion is defined as:

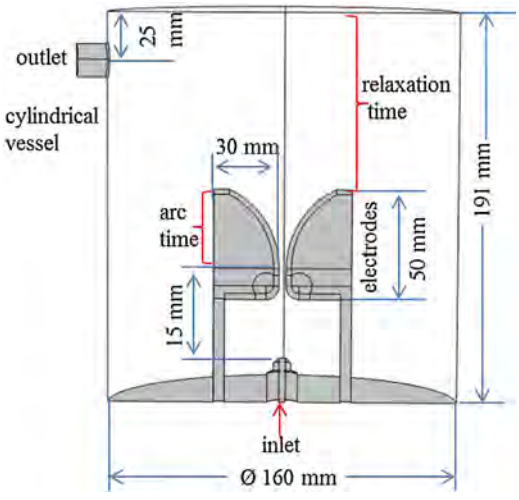

Fig. 1. Schematic illustration of the experimental GA reactor.

$$X_{CO_2}(\%) = \frac{CO_{2,\,inlet} - CO_{2,\,outlet}}{CO_{2,\,inlet}} \times 100\% \quad (1)$$

while the energy efficiency is determined by

$$\eta(\%) = \frac{X_{CO_2}(\%) \cdot \Delta H(\mathrm{kJ/mol})}{\mathrm{SEI(kJ/L)} \cdot 22.4(\mathrm{L/mol})} \times 100\% \quad (2)$$

$$\mathrm{SEI(kJ/L)} = \frac{\mathrm{Power(kW)}}{\mathrm{Flow\ rate(L/min)}} \times 60(\mathrm{s/min}) \quad (3)$$

where ΔH is the reaction enthalpy of pure CO_2 decomposition (279.8 kJ/mol) and the input power is recorded by a power meter (Maplin, L61AQ).

3. Description of the 0D model and chemical reactions considered in the model

The model used for this study is a 0D chemical kinetics model, called ZDPlaskin [71]. In this model, the time-evolution of the species densities is calculated by balance equations, taking into account the various production and loss terms by chemical reactions. Because the model is 0D, transport processes are not considered explicitly, but the transport of the arc and the effect of the gas flowing through the GA reactor are accounted for, as explained in Section 4 below. The coupled ordinary differential equations are expressed in the following form:

$$\frac{dn_i}{dt} = \sum_j [(a_{ij}^R - a_{ij}^L) k_j \prod_l n_l^L] \quad (4)$$

where n_i is the density of species i, a_{ij}^R and a_{ij}^L are the right-hand side and left-hand side stoichiometric coefficients of species i in the reaction j, k_j is the reaction rate constant and n_l^L is the density of the lth reactant of reaction j. Energy is supplied to the plasma electrons by the applied electric field, and the electron temperature is calculated by the Boltzmann equation solver using the local field approximation for different reduced electric field values E/N (see below). This reduced electric field is calculated at each time step, to keep the desired power density due to the changing gas composition as a function of time.

In this model, we don't calculate the gas temperature self-consistently, but we assume a certain gas temperature as input, based on experimental measurements from literature, and we also discuss the influence of gas temperature on the conversion and energy efficiency in Section 5.3. In [58] the gas temperature was measured for the dry reforming of methane process in a rotating gliding arc reactor. The dependence of the gas temperature on the applied voltage was investigated for a CH_4/CO_2 mixture of 3/7. By increasing the applied voltage from 7 kV to 10 kV, the gas temperature only increased by 10%, i.e., from 1080 K to 1180 K. This implies that the GA discharge maintains high selectivity in channeling the energy into products rather than into loss by enthalpy. Therefore, the gas temperature is assumed in our model to be 1200 K in the arc region, based on these measurements, and when the gas leaves the arc column, the gas temperature is assumed to drop to 500 K, which is measured at the outlet in our experiments.

The chemical species considered in this model are presented in Table 1. These species include various neutral molecules in the ground state, as well as in several electronically and vibrationally excited levels, various radicals, positive and negative ions, and the electrons. In total, 72 species are taken into account. The symbols

Table 1
Species included in the model, besides the electrons.

Ground state molecules	CO_2, CO, O_2, O_3
Radicals	C_2O, C_2, C, O
Electronic states	$CO_2(e)$, $CO(e_1)$, $CO(e_2)$, $CO(e_3)$, $CO(e_4)$, $O_2(e_1)$, $O_2(e_2)$
Vibrational states	$CO_2(V_a)$, $CO_2(V_b)$, $CO_2(V_c)$, $CO_2(V_d)$, $CO_2(V_1)\cdots CO_2(V_{21})$, $CO(V_1)\cdots CO(V_{10})$, $O_2(V_1)$, $O_2(V_2)$, $O_2(V_3)$, $O_2(V_4)$
Positive ions	CO_2^+, CO^+, CO_4^+, O_2^+, O^+, O_4^+, $C_2O_2^+$, $C_2O_3^+$, $C_2O_4^+$,C_2^+,C^+
Negative ions	CO_3^-, CO_4^-, O_2^-, O^-, O_3^-, O_4^-

"V" and "e" between brackets for CO_2, CO and O_2 represent the vibrationally and electronically excited levels of these species, respectively. Special attention is paid to the vibrational levels of CO_2, and more specifically to the levels of the asymmetric stretch mode, denoted here as V(1–21), as they are expected to play an important role in energy-efficient CO_2 conversion, based on our experience for a MW plasma [67,68,72]. More details about all the excited levels, and an explanation about the meaning of the notations in Table 1, can be found in [67,68].

The chemical reactions used in the model include electron impact reactions, vibrational energy transfer reactions, and chemical reactions between the various neutral species and the various charged species, which are presented in detail in [67,68] and updated in [73]. For the electron impact reactions, a cross-section database, adopted from LxCat [74], is given as input to the Boltzmann equation solver BOLSIG+ [75], which calculates the electron energy distribution function (EEDF) for different values of reduced electric fields. Subsequently, the rate constants of the various electron impact reactions can be obtained from this EEDF and the cross sections. Note that for electron impact excitation-dissociation, the excitation cross section by Phelps with 7 eV threshold is adopted, as recommended in [76].

For the vibrational energy transfer reactions, three types can be distinguished: (i) vibrational energy transfer to the translational degrees of freedom, i.e., VT relaxation, (ii) vibrational energy transfer between the symmetric and asymmetric mode levels of CO_2, i.e., VV' relaxation, and (iii) vibrational energy transfer among two molecules in the same mode of vibration, i.e., VV relaxation. The rate constants of the heavy particle reactions are assumed to be only a function of the gas temperature and are adopted from the literature (see details in [67,68,72,73]).

The calculated CO_2 conversion is defined as follows:

$$X_{CO_2}(\%) = \left(1 - \alpha \frac{n_{CO_2,tot}(t_r)}{n_{CO_2,tot}(0)}\right) \times 100\% \quad (5)$$

where $n_{CO2,tot}$ is the total calculated CO_2 density (including ground state and excited levels), t_r denotes the gas residence time (defined in Section 4 below) and 0 stands for the start of the simulation, corresponding to the position of the gas inlet. In the model the concentration of the species only varies as a function of time. This temporal variation can, however, easily be translated into a spatial variation in the GA reactor, i.e., when the gas molecules travel from the inlet to the outlet, by means of the gas flow rate. In other words, the variation of the species concentrations as a function of time (in the model) is the same as the variation as a function of position (in reality).

Because the CO_2 gas is gradually converted into CO and O_2 molecules when travelling through the GA reactor, the number of molecules will increase, or in other words, the gas volume will expand for the same inlet gas flow rate. Therefore, a correction factor (α) has to be incorporated, to account for this gas expansion. This correction factor is expressed as the ratio of the gas species fluxes at the exit vs the inlet [77]. Because CO_2 is partially converted into CO and O_2, there will be more molecules at the exit compared to at the inlet, yielding a value of $\alpha > 1$, depending on the actual conversion.

To calculate the energy efficiency of the CO_2 conversion, we define the specific energy input (SEI):

$$\mathrm{SEI(eV/molecule)} = \frac{P(\mathrm{W})}{eQ_n(\mathrm{s^{-1}})} \quad (6)$$

Where e links the units of J to eV ($1\,\mathrm{eV} = 1.6 \times 10^{-19}\,\mathrm{J}$), Q_n is the particle flow rate (in number of molecules per second), defined by Eq. (7):

$$Q_n(s^{-1}) = \frac{p(\mathrm{Pa})}{k_B(\mathrm{J/K})T_{gas}(\mathrm{K})10^6(\mathrm{cm^3/m^3})} \cdot Q_{gas}(\mathrm{cm^3/s}) \quad (7)$$

Furthermore, P is the plasma power (W), p is the gas pressure (Pa), k_B is the Boltzmann constant (J/K), T_{gas} is the gas temperature (K), and Q_{gas} is the inlet gas flow rate (expressed here in $\mathrm{cm^3\,s^{-1}}$). The factor 10^6 is used to transfer the units of $\mathrm{m^3}$ to $\mathrm{cm^3}$.

Subsequently, the energy efficiency (η) is calculated as:

$$\eta(\%) = X_{CO_2}(\%) \cdot \frac{\Delta H(\mathrm{eV\ /\ molecule})}{\mathrm{SEI(eV\ /\ molecule)}} \quad (8)$$

With ΔH the reaction enthalpy for CO_2 splitting ($CO_2 \rightarrow CO + 1/2O_2$), i.e., 279.8 kJ/mol (see also previous section) or 2.9 eV/molec.

4. Application of the 0D model to a GA discharge

Although it is reported in literature that the arc undergoes a transition from thermal to non-thermal regime when dragged by the gas flow to larger interelectrodes gap [61], this typically applies to a GA operating at higher currents than the conditions under study here. Indeed, at the conditions under study here, both our 2D and 3D simulations [65,66], as well as the experiments [69,70], indicate that the gliding arc is only in the non-thermal regime from the ignition at the shortest gap. Therefore, in this simulation, we do not consider the transition from thermal to non-thermal region, and we treat the GA as a non-thermal plasma. The 0D model is applicable to the non-equilibrium region, and although a 0D model cannot describe the increase of arc length from short arc at the shortest gap to long arc at a larger gap, we can use the time evolution of the plasma parameters as input, which are related to the increase of arc length during the arc downstream movement.

As mentioned above, a 0D model only calculates the species densities as a function of time, and transport processes are not explicitly considered. Nevertheless, the transport of the arc through the GA reactor can be mimicked by translating the temporal behavior, as calculated in the model, into a spatial behavior, corresponding to the position in the reactor, by means of the gas flow rate. We thus need to specify how the spatial variations in the reactor, more specifically for the power density, can be translated into temporal variations, to be used as input in the model. The power density is assumed to be constant in the region between the electrodes where the arc is formed (cf. Fig. 1 above; also called "arc time" in the model). This constant value is justified, although we know that the arc length increases with time

and position, but in reality also the electric power increases with time and position, so the electric power per unit length can be considered constant during the arc movement. Moreover, the radius of the plasma string will also remain constant during the arc movement, as observed in experiments [78,79], so the power density can indeed be considered constant.

Furthermore, it is reported in literature that the gliding arc is a plasma string with a diameter of about 1 mm, surrounded by a weakly ionized zone [78,79]. This can also be clearly seen from our 3D calculation results in Fig. 2.

Thus, in our 0D model the arc volume is seen as a cylinder with a diameter of about 1 mm, and the power density in the arc zone (i.e., the region between the electrodes) is calculated as the plasma power divided by the arc volume. We apply the same power as in the experiments, i.e., between 70 and 100 W (see Section 5 below). The arc diameter will slightly increase with plasma power, and thus we assume the arc radius to be 0.5, 0.525, 0.55 and 0.575 mm in our model, at a power of 70, 80, 90 and 100 W, respectively. Therefore, the initial arc volume is calculated to be 1.96×10^{-3}, 2.17×10^{-3}, 2.38×10^{-3} and 2.59×10^{-3} cm^3 for these power values, respectively, yielding a power density of 3.56×10^4, 3.69×10^4, 3.78×10^4 and 3.85×10^4 W/cm^3 in the plasma power range of 70–100 W. When a power density of 3.85×10^4 W/cm^3 is applied, the electron density calculated in our 0D model is around $(4.5–5) \times 10^{12}$ cm^{-3} in the arc zone, as shown in Fig. 3, which is comparable to the electron density measured in a low current (0.1 A) air gliding arc [80]. Note that the electron density plotted in Fig. 2 is about 10^{14} cm^{-3} for a low current GA plasma, but this was obtained in argon, and it is expected that the electron density in a CO_2 discharge is lower, due to electron attachment and the formation of negative ions [81]. Finally, this power density yields a calculated electron temperature of 1.8–2.0 eV, as also presented in Fig. 3, and this is also in agreement with the experimentally measured electron temperature range of 1–2 eV [58,82]. In the region beyond the electrodes (cf. Fig. 1, called the "relaxation time" in our model), the power density is zero, and thus, both the electron density and electron temperature also drop to zero, as is clear from Fig. 3.

Furthermore, it is known that only a small fraction of the inlet gas (10–20%) can pass through the discharge zone in a conventional GA [83–85]. Our previous 2D modeling results [66] have pointed out that the velocity of the moving arc differs to some extent from the gas flow velocity, due to the phenomenon of back-breakdown, which is characteristic for a conventional GA discharge. This process is illustrated in Fig. 4, and it results in a somewhat larger fraction of the gas that can pass through the arc and be treated, compared to the situation where the arc would move with the same velocity as the gas flow velocity. Therefore, in our model, the fraction of the treated gas is assumed to be 20%, and the inlet gas is divided in two parts, i.e., 80% will not be processed and 20% passes through the arc zone. The final gas composition at the outlet will be the result of the two flows mixing downstream of the discharge.

The gas processing time in the arc is assumed to be 8 ms, which is deduced from the voltage signal in the experiments, i.e., the arc voltage suddenly drops after 8 ms, indicating that a new arc cycle occurs [69,70]. After this, the treated gas leaves the arc region, and

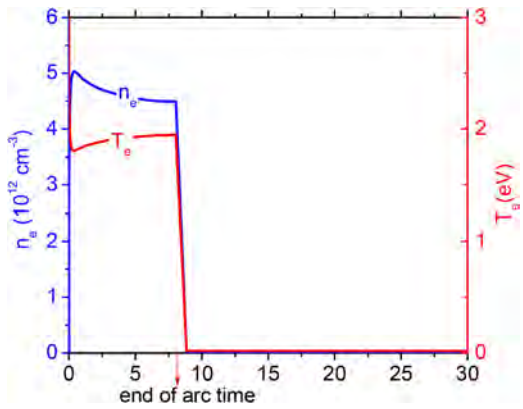

Fig. 3. Calculated electron temperature (red line; right y-axis) and electron density (blue line; left y-axis) as a function of time during (and after) the arc. (For interpretation of the references to colour in this figure legend, the reader is referred to the web version of this article.)

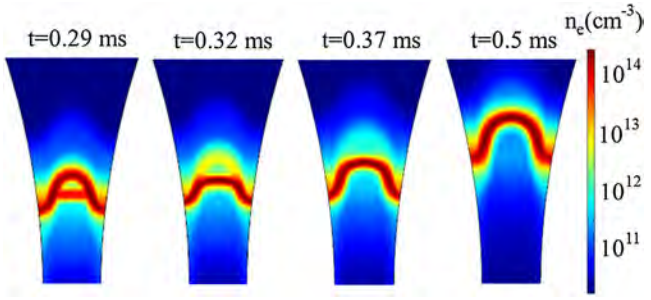

Fig. 4. Time-evolution of the electron density, calculated with our 2D model for an argon GA discharge, illustrating how the arc expands when it travels from short to larger interelectrode distance, as well as the back-breakdown event, where a new breakdown occurs following a shorter path between both electrodes [66].

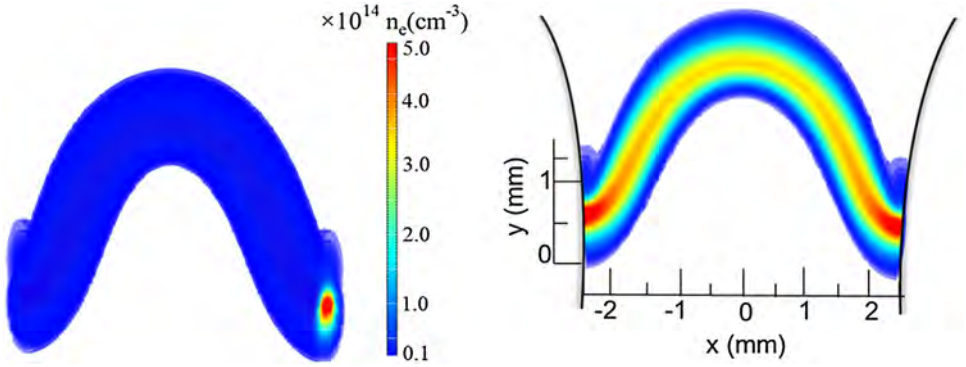

Fig. 2. Illustration of a typical electron density profile in one arc, calculated with our 3D model for an argon GA discharge [66]. Note that the right figure is the cross section of the left figure, to illustrate the interior of the arc. In the right figure, the electrodes between which the arc is formed are schematically illustrated (cf. Fig. 1), and the dimensions of the arc are given.

enters the relaxation zone, as shown in Fig. 1 above. Subsequently, the new arc will process the new incoming gases at the shortest interelectrode gap, and this process repeats itself.

Besides the gas processing time, we also need to define the total gas residence time in the reactor. The gas flow rate is fixed at 6.5 L/min. This yields an average axial gas flow velocity of 11 m/s, as simulated by the so-called k-ω RANS turbulent modeling technique in a 3D model. Based on the reactor length of 191 mm (see Fig. 1 above), the calculated average gas flow time along the reactor length is about 17.4 ms. As this is an average, and some molecules might spend a longer time in the reactor, we set the total gas residence time in our calculations as 30 ms, which is sufficient, because the gas composition does not change with time anymore, as will be shown in Section 5.2, so it has no influence on the conversion.

To summarize, the simulation is divided in two phases, as shown in Fig. 1, i.e., the arc processing phase and a relaxation phase. In the first phase, the electrons are heated by the electric field and they activate the gas molecules. This applies to the gas passing through the arc column (see above). In the second phase, which starts at 8 ms, the power deposition goes to zero, and as a result, also the electron density and temperature drop to zero (see Fig. 3), and the reacting species are given time to relax to equilibrium.

5. Results and discussion

5.1. CO_2 conversion and energy efficiency

A comparison between the calculated and measured CO_2 conversion and energy efficiency as a function of discharge power and shortest interelectrode gap is illustrated in Figs. 5 and 6, respectively. The conversion is typically between 6 and 10%, for the different conditions investigated, while the corresponding energy efficiency is around 20–40%. These values will be benchmarked against other results from literature, for various types of plasma reactors, in Section 5.4 below.

As is clear from Fig. 5, the calculated and measured CO_2 conversion increase with increasing electrical power. As expected, a higher electrical power yields a higher electron density, and thus a higher density of vibrationally excited states of CO_2, which promotes the CO_2 dissociation, as will be shown in the next section. The measured and calculated energy efficiency, on the other hand, slightly drop with increasing power. This can be explained from Eqs. (2) and (8) above. Indeed, the energy efficiency rises linearly with the conversion, but is also inversely proportional to the SEI. Hence, if the conversion rises less rapidly than the SEI (which is determined by the power, keeping the flow rate constant), this will result in a drop in the energy efficiency as a function of the SEI. As is clear from Fig. 5, an increase in the plasma power by a factor 1.4 results in a rise in the conversion by only a factor 1.2. Hence, this explains why the energy efficiency slightly drops upon increasing power (or SEI). A good agreement is reached between experimental and calculated data, although the calculated energy efficiency is slightly lower than the experimental values. In fact, the agreement between calculations and experiments is already very satisfactory, certainly in view of the fact that the coupling interaction of the gas flow with the arc is a complex process in a GA discharge, which cannot be fully captured by a 0D model.

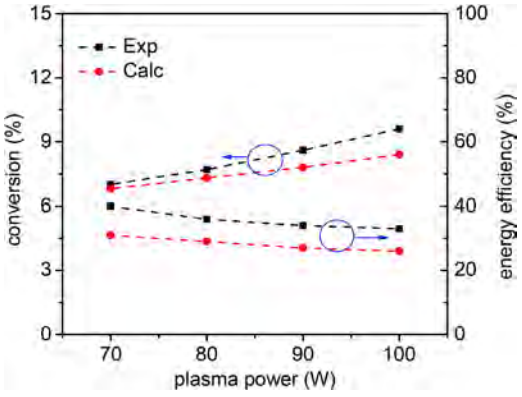

Fig. 5. Experimental and calculated values of CO_2 conversion and energy efficiency as a function of plasma power, at a gas flow rate of 6.5 L/min and a shortest interelectrode gap of 2.5 mm.

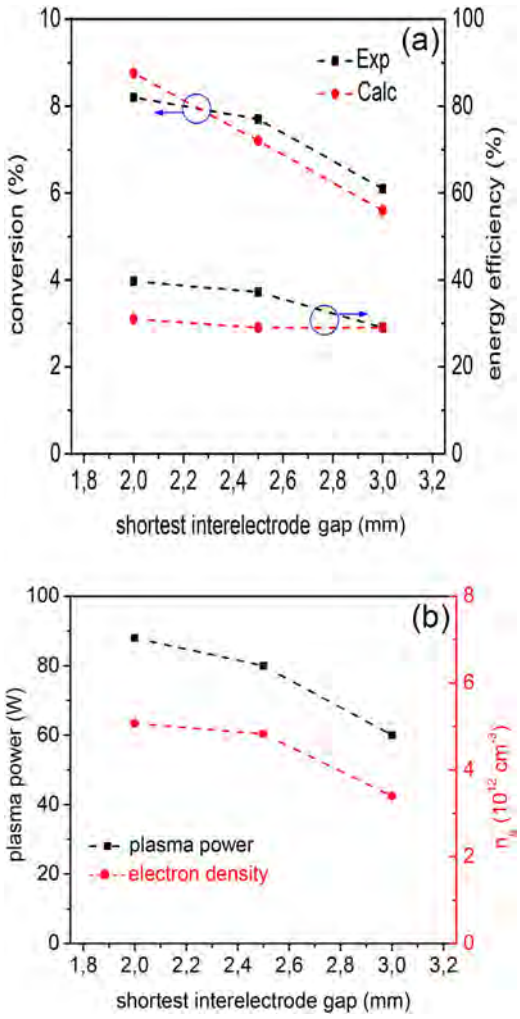

Fig. 6. Experimental and calculated values of CO_2 conversion and energy efficiency (a), and electron density and plasma power in the GA discharge (b), as a function of the shortest interelectrode gap, for a gas flow rate of 6.5 L/min.

The influence of the shortest interelectrode gap on the calculated and measured conversion and energy efficiency is presented in Fig. 6(a). A larger interelectrode gap results in a drop in both the experimental and calculated conversion, while the energy efficiency drops only slightly in the experiments and remains more or less constant in the calculated results.

This drop in conversion can be explained because a larger interelectrode gap results in a slight increase of the arc volume, and in a decrease of the plasma power measured from the electrical signals, thus resulting in a somewhat lower electron density, as both shown in Fig. 6(b). This lower electron density results in a drop in electron impact reaction rates, explaining the drop in CO_2 conversion. As the energy efficiency depends on the conversion

and the power (or SEI; cf. Eqs. (2) and (8) above), which both drop upon larger interelectrode gap, this also explains why the energy efficiency drops only slightly or remains more or less constant.

We can conclude from Figs. 5 and 6 that our model shows the same trends as the experimental data, for different conditions, and also the absolute values are in reasonable agreement. Therefore, we believe that the model is sufficiently realistic to be used to elucidate the underlying chemical mechanisms of CO_2 splitting, which will be presented in the next section.

5.2. Reaction products and chemical reaction pathway analysis for CO_2 conversion

In this section, the underlying plasma chemistry mechanisms for the CO_2 conversion in the GA discharge will be discussed. Indeed, a better insight into the dominant chemical reactions might help to steer the process to improve the CO_2 conversion and energy efficiency.

The time evolution of the most important neutral species densities is presented in Fig. 7. The densities of CO_2, CO, and O_2 represent the total densities, including the electronic and vibrationally excited states. At the initial stage, i.e., in the first 0.1 ms, the densities of CO and O increase together (see Fig. 7(a)), due to the electron impact dissociation reaction $CO_2 + e \rightarrow CO + O + e$. After about 0.1 ms, the density of the O atoms rises more slowly than the CO density, and at the same time, the density of the O_2 molecules rises, because the O atoms recombine into O_2 molecules. A small fraction of the O atoms will also recombine with O_2 molecules, yielding the production of O_3, but their density is several orders of magnitude lower, as is clear from Fig. 7.

After the gases have passed through the arc region, the relaxation phase begins, as indicated by the black dashed vertical line in Fig. 7(b). Strikingly, the O atom density abruptly decreases, while the O_2 and O_3 densities increase, indicating that the O atoms are rapidly converting into O_3 and O_2. Furthermore, also the CO_2 density, which showed a decreasing trend in the arc phase, now recovers to more or less its initial value, due to the sudden drop of gas temperature to 500 K after leaving the arc zone at constant pressure. Indeed, inside the arc phase, the CO_2 density drops from the initial value of $6.1 \times 10^{18}\,cm^{-3}$ to $3.1 \times 10^{18}\,cm^{-3}$, yielding a conversion of 34%, taking into account the gas expansion factor at constant pressure. However, immediately after the arc phase, it rises again due to the gas temperature drop, and then stays constant in the relaxation phase. This means that the relaxation phase does not contribute to the CO_2 conversion, not in the positive direction (contributing to more CO_2 dissociation), nor in the negative direction (i.e., the reverse – recombination – reactions between CO and O atoms are also negligible in the relaxation phase due to the low temperature; see below). Finally, by mixing with the 80% untreated CO_2 gas, the overall CO_2 conversion over one arc cycle is only limited to 6.8% at the conditions under study (cf. also Fig. 5 above). The product distribution at the end of the relaxation phase, being mainly CO and O_2, at a ratio of 2.05, is the same as for the experimentally measured products at the outlet, and was also reported by others in literature [49]. The underlying chemistry of the conversion process will be discussed in the reaction pathway analysis below.

The most important reactions responsible for the CO_2 conversion, integrated over the entire gas residence time, are presented in Fig. 8. As mentioned above, the conversion only takes place during the arc phase, because the temperature in the relaxation phase is too low, and the power (and electron density and temperature) have dropped to zero. The main reaction in the entire power range is electron impact dissociation of vibrationally excited states of CO_2 into CO and O, with a relative contribution of about 61–67%, slightly decreasing upon increasing power. Besides, electron impact dissociation of ground state CO_2 into CO and O, as well as CO_2 dissociation upon collision with ions, also contribute each by about 10%. Furthermore, upon increase of the plasma power, also the dissociation of vibrationally excited states of CO_2 upon collision with any neutral species (M) or specifically with the O atoms, become slightly more important, reaching a contribution up to 10% and 7%, respectively, at a plasma power of 100 W. The

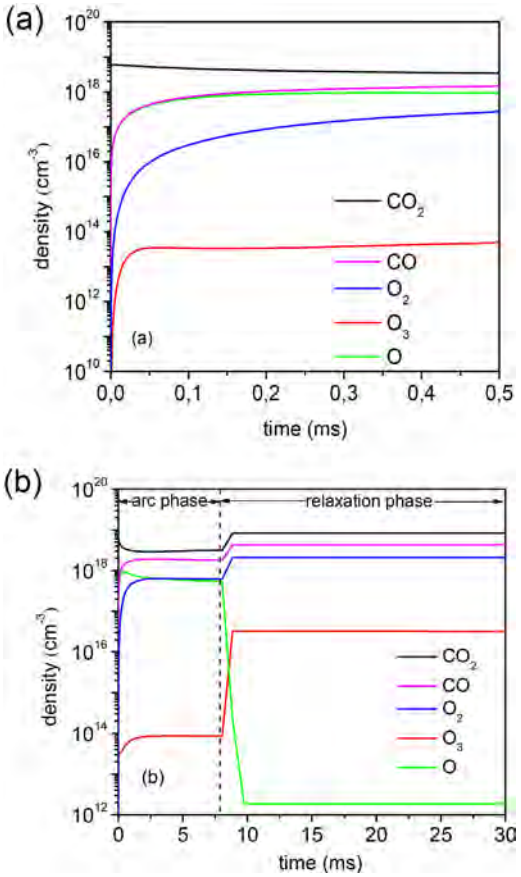

Fig. 7. Time evolution of the most important neutral species densities, at a plasma power of 70 W, a gas flow rate of 6.5 L/min and a shortest interelectrode gap of 2.5 mm. Panel (a) shows the details in the first 0.5 ms, while panel (b) shows the overall evolution in the arc phase and relaxation phase.

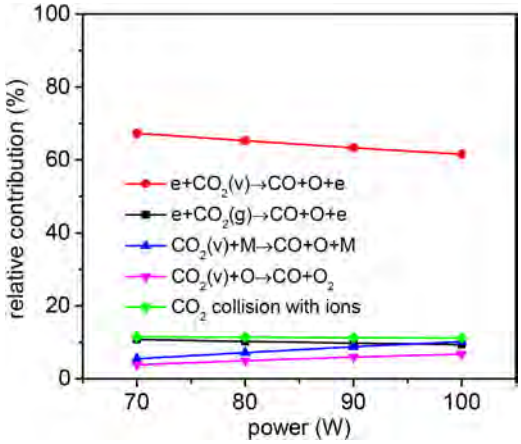

Fig. 8. Relative contributions of the most important reactions responsible for the CO_2 conversion, integrated over the entire gas residence time, as a function of plasma power.

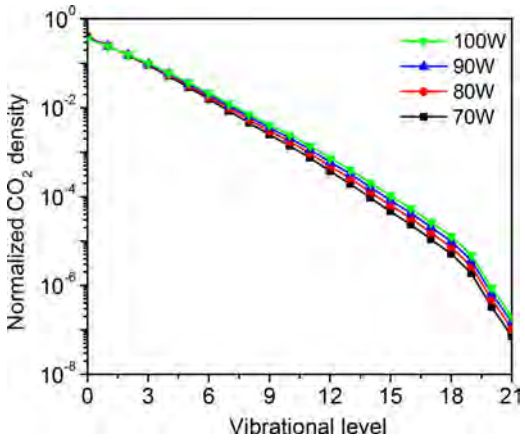

Fig. 9. Normalized vibrational distribution functions of the asymmetric mode of CO_2 at the end of the arc phase (t = 8 ms) and different values of the plasma power.

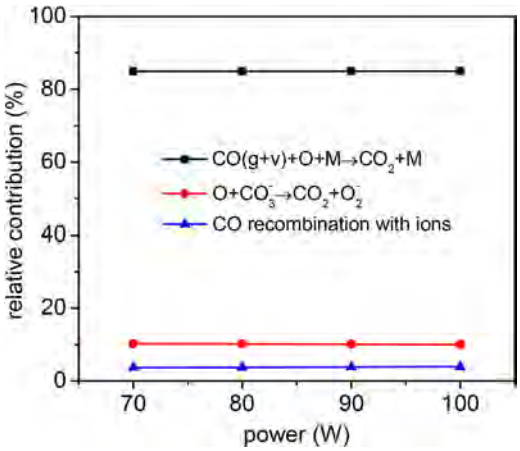

Fig. 10. Relative contribution of the most important formation processes of CO_2, integrated over the entire gas residence time, as a function of plasma power.

specific CO_2 destruction processes will be shown in detail in the reaction pathway analysis below.

It is clear that the vibrational levels of CO_2 play a crucial role in the CO_2 splitting process. In Fig. 9, the normalized vibrational distribution functions (VDFs) of the asymmetric mode of CO_2, obtained at a time of 8 ms (i.e., the end of the arc phase), are depicted for four different power values.

The populations of the higher vibrational levels slightly increase with the plasma power, and this explains why the CO_2 conversion increases with plasma power, since the dissociation of CO_2 upon collision with any neutral species (M) or with the O atoms mainly proceeds through these higher vibrational levels. Indeed, these higher asymmetric mode vibrational levels (V(11)–V(21)) account for 99.9% and 98.5% of the dissociation of CO_2 upon collision with any neutral species (M) and with the O atoms, respectively, at a plasma power of 100 W. Moreover, the electron density also increases with rising power, and all this explains the higher CO_2 conversion upon rising power. Note that electron impact dissociation of the vibrationally excited states of CO_2 mainly proceeds from the lower asymmetric mode levels and from the symmetric mode levels, which have a high enough density for this process to occur. In fact, the symmetric mode vibrational levels (V(a)–V(d) in Table 1) account for 73% of the total electron impact vibrational dissociation in our model, while the relative contributions of the lowest three asymmetric mode vibrational levels (V(1)–V(3)) amount to 21%, and the other asymmetric mode vibrational levels only account for 6% at a plasma power of 100 W. Although the higher asymmetric mode vibrational levels only play an important role in the dissociation of CO_2 upon impact with any neutral species (M) or with the O atoms, which only have a small contribution to CO_2 conversion at the conditions under study (i.e., up to 10 and 7%, respectively; cf. Fig. 8 above), the higher vibrational levels are still quite important for CO_2 conversion in a GA discharge, and their importance also depends on the discharge conditions, which will be shown in Section 5.3.

Besides dissociation of CO_2, some of the reactions plotted in Fig. 8 also occur in the opposite direction, giving rise to the formation of CO_2 again. The most important reactions for CO_2 formation are plotted as a function of plasma power in Fig. 10. The reaction of CO (either in the ground states or in vibrationally excited states) with O atoms and a third body (M) is the predominant production process of CO_2, with a relative contribution to the overall CO_2 formation amounting to 85% at all plasma powers investigated. Furthermore, the reaction of O atoms with CO_3^- ions also plays a non-negligible role in the CO_2 formation, contributing for about 10% in the entire power range. Other reactions that play a minor role towards CO_2 formation (<5%) include CO recombination with ions, and to a lower extent also the recombination between positive and negative ions, and O atom recombination with ions (not shown in Fig. 10). These reaction paths will be presented in detail in Fig. 11 below. Note that the reverse reactions, especially the three-body recombination of CO with O atoms, have a detrimental effect on the CO_2 conversion. Indeed, when this reaction rate becomes large enough, it will inhibit further CO_2 dissociation. This might happen at the end of the arc phase, when a considerable fraction of the CO_2 molecules is already converted into CO and O.

From the above analysis, we can compose an overall reaction scheme of CO_2 splitting and formation, as presented in Fig. 11. This allows us to identify in more detail the reactions that should be targeted in our aim to further improve the CO_2 conversion. The dominant CO_2 loss mechanism is dissociation upon collision with electrons (e), forming CO and O, as appears from the thickest arrow

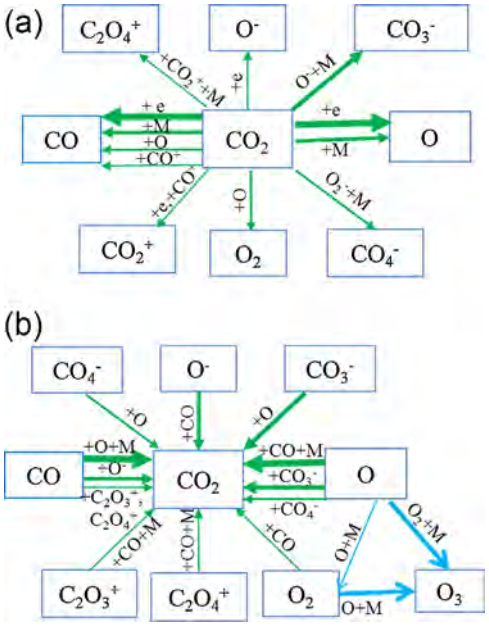

Fig. 11. Reactions pathways illustrating the CO_2 splitting (a) and formation (b) mechanisms. The thickness of the arrow lines corresponds to the importance of the reactions. The conversion reactions between O, O_2 and O_3 are also indicated in (b), with blue arrow lines. (For interpretation of the references to colour in this figure legend, the reader is referred to the web version of this article.)

line, and as could also be deduced from Fig. 8 above. In Fig. 11, no distinction is made between CO_2 molecules in the ground state or vibrationally excited levels, but it is clear from Figs. 8 and 9 that the major contribution arises from the CO_2 lower asymmetric and symmetric mode vibrational levels. Another important loss mechanism is dissociation of CO_2 upon collision with any heavy species (M), forming CO and O; see also Fig. 8 above. The other loss processes illustrated in Fig. 11 represent CO_2 dissociation upon impact with O atoms and dissociative electron attachment, forming CO and O_2, or CO and O^-, respectively, as well as several reactions with ions, as shown in detail in Fig. 11(a). Among these ion reactions, the most important loss mechanism is dissociation of CO_2 upon collision with negative ions O^- (and M atoms), forming CO_3^-. All these ion reactions together contribute for only about 10% to the CO_2 loss, as indicated in Fig. 8.

Most of the ions, however, also contribute to the CO_2 formation, as described in detail in Fig. 11(b), so the net role of the ion reactions in the CO_2 loss or formation is not very important. The ions playing a role in the CO_2 formation include O^-, $C_2O_3^+$ and $C_2O_4^+$, reacting with CO to form CO_2, as well as CO_4^- and CO_3^-, reacting with O atoms to CO_2. However, the contribution of these ions to the CO_2 formation is again only about 10–15%, as indicated in Fig. 10 above. If we want to improve the CO_2 conversion, it is better to intervene in the dominant CO_2 formation process, being the recombination reactions of CO with O atoms and a third body (M) (cf. the thickest arrow lines in Fig. 11(b)), which has a contribution of about 85% (cf. Fig. 10). This will be elaborated in the next section.

During the arc phase, the O atom density is very large, as shown in Fig. 7, but in the relaxation phase, the O atom density abruptly decreases, and there is almost no O measured at the reactor outlet. Hence, the above recombination reaction between CO, O and a third body will only be substantial during the arc phase. The reason why the O atom density becomes negligible in the relaxation phase is because the gas temperature sharply drops to 500 K when the gas leaves the arc zone and enters the relaxation zone. As a consequence, the rate coefficient of the three-body reaction between O atoms and O_2 molecules, forming O_3, increases, as it is strongly temperature dependent: $k = 6.11 \times 10^{-34}(T_g/300)^{-2.6}\mathrm{cm^6 s^{-1}}$. Hence, this three-body reaction of O with O_2 becomes the most important loss process for the O atoms, which can also be deduced from the sharp increase of the O_3 density, presented in Fig. 7(b) above. Furthermore, two O atoms will also recombine into the formation of O_2, as illustrated in Fig. 11(b).

From this analysis we can conclude that a lower gas temperature inside the arc phase could reduce the density of O atoms by converting them to O_3 and O_2, which may prevent the reverse reaction of O and CO into CO_2, and thus improve the CO_2 conversion. Therefore, in the following section, we will firstly investigate the influence of gas temperature in the arc on the conversion and energy efficiency of CO_2, before elaborating on other possible ways to improve the CO_2 conversion.

5.3. How to improve the CO_2 conversion and energy efficiency in a GA discharge?

5.3.1. Effect of the gas temperature

From the discussions above, it is clear that, in order to increase the CO_2 conversion, we have to inhibit or reduce the formation of CO_2 upon recombination between CO and O, and the most obvious and direct method would be to lower the gas temperature inside the arc, so that O recombines faster into O_3 (cf. above). Moreover, a lower gas temperature will result in a lower reaction rate coefficient of the three-body recombination of CO and O.

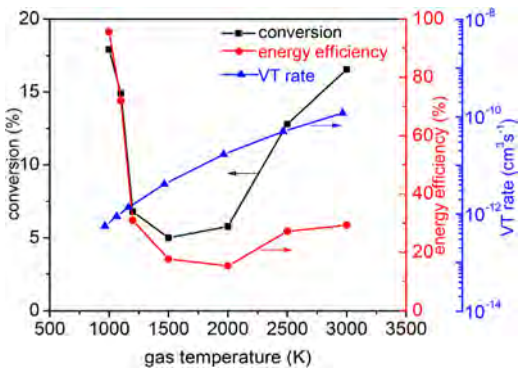

Fig. 12. Calculated CO_2 conversion, energy efficiency and VT relaxation rate as a function of gas temperature inside the arc, at a plasma power of 70 W, a gas flow rate of 6.5 L/min and a shortest interelectrode gap of 2.5 mm.

Therefore, we investigate here the effect of different gas temperature values inside the arc, on the conversion and energy efficiency of CO_2.

As is obvious from Fig. 12, in the gas temperature range of 1000–1500 K, the conversion and energy efficiency of CO_2 decrease dramatically with increasing gas temperature. At a gas temperature of 1000 K, both the conversion and energy efficiency are very high, reaching up to 18% and almost 96%, respectively. This can be explained from the reduced reverse reaction of CO and O into CO_2, because the O atoms more easily recombine with O_2 and O_3 at low temperature (see above), but also from the VDF, plotted in Fig. 13 (see discussion below).

When the gas temperature inside the arc increases to 1200 K and further to 1500 K, both the conversion and energy efficiency exhibit a significant drop to 5% and 18% respectively. When further increasing the temperature to 2000 K, the conversion and energy efficiency are virtually unaffected, but a further increase from 2000 K to 2500 K, and even to 3000 K results in a significant rise in the CO_2 conversion up to 16.5% at 3000 K, while the energy efficiency rises only slightly, i.e., up to 29.3% at a gas temperature of 3000 K. In this high gas temperature range, the slight increase of the energy efficiency at high gas temperatures, i.e., 2500 and 3000 K, is caused by the increase of the CO_2 conversion. At high gas temperature, the SEI value also increases, i.e., every molecule is getting more energy, but when the CO_2 conversion rises more rapidly than the SEI, this will result in an increase of the energy efficiency as a function of the gas temperature (cf. Eq. (8) above).

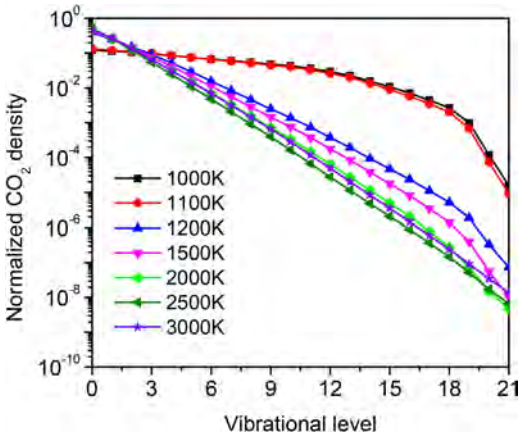

Fig. 13. Normalized vibrational distribution functions of the asymmetric mode of CO_2 in the GA discharge at t = 8 ms, for different gas temperature values inside the arc, at a plasma power of 70 W, a gas flow rate of 6.5 L/min and a shortest interelectrode gap of 2.5 mm.

From Fig. 12, we can see that when the gas temperature rises from 1500 to 2000 K, the conversion rises only to some extent, so the energy efficiency slightly drops. However, when increasing the gas temperature to 2500 and 3000 K, the conversion rises significantly, resulting in a slight increase of the energy efficiency. The plasma is in the high gas temperature only a heater, i.e., a provider of the required high temperature [10]. Hence, in this regime the advantages of the selective, non-equilibrium vibrational excitation of CO_2 are suppressed. In Fig. 12 we also plot the VT relaxation rate ($CO_2v_2 + M \rightarrow CO_2v_1 + M$); see blue curve and right y-axis. We can clearly see that the VT rate increases with gas temperature, resulting in a lower density of high vibrational levels at high gas temperatures.

Fig. 13 presents the effect of gas temperature on the normalized VDF of the asymmetric mode of CO_2. At 1000 and 1100 K, the VDF looks strikingly different from the VDFs at the higher temperatures, with much higher densities of the higher vibrational levels. When the gas temperature rises to 1200 K and higher, the VDF drops steeply towards higher vibrational levels. From the slope of the VDFs, we can deduce a so-called vibrational temperature, assuming a Maxwellian distribution ($N \sim \exp(-eE/kT_{vib})$ [72]). At 1000 and 1100 K, there is not a single slope in the VDF, illustrating that the VDF does not follow a Maxwellian distribution, which points towards thermal non-equilibrium. Instead, three slopes can more or less be distinguished, and the corresponding vibrational temperatures are 25000 K, 6600 K and 1280 K for the gas temperature of 1000 K, while they are 22000 K, 6200 K, 1237 K for the gas temperature of 1100 K. These values are much larger than the gas temperature of 1000 and 1100 K, especially for the first and second group of levels, thus indeed clearly pointing towards thermal non-equilibrium. At the higher gas temperatures, the VDFs can be represented by an exponentially decaying function, and from the slopes in Fig. 13, we can deduce vibrational temperatures of 7000 K, 5900 K, 5000 K, 4400 K and 4800 K, at the gas temperatures of 1200 K, 1500 K, 2000 K, 2500 K and 3000 K, respectively. Hence, the ratio of T_{vib}/T_g decreases from 5.8 to 1.6. Thus, it is clear that the VDFs indeed become close to thermal equilibrium upon higher gas temperature.

Our calculations predict that the lower asymmetric mode levels and the symmetric mode levels, which have a higher density, are mainly contributing to the CO_2 dissociation at a temperature of 1200 K and above. In the gas temperature range of 1200–2000 K, electron impact dissociation of vibrationally excited states of CO_2 is the main loss process, in which the lower asymmetric mode levels and the symmetric mode levels play the most important role. When further increasing the gas temperature from 2000 K to 2500 K, and even to 3000 K, the dissociation of vibrationally excited states of CO_2 upon collision with the O atoms becomes more and more important, and again the lower asymmetric mode levels and the symmetric mode levels play the most important role. If we take the gas temperature of 3000 K as an example, we can conclude that the dissociation of the vibrationally excited states of CO_2 upon collision with O atoms is the most important splitting process. The relative contributions of the symmetric mode vibrational states to the CO_2 dissociation amount to 72%, while the lowest five vibrational levels of the asymmetric mode (V(1)–V(5)) account for 20%, the intermediate asymmetric mode vibrational levels V(6)–V(10) account for 6%, and the highest asymmetric mode levels V(11)–V(21) contribute for only 2% to this CO_2 dissociation process.

On the other hand, at a gas temperature of 1000 K, dissociation of the high vibrationally excited states of CO_2 upon collision with any neutral species (M) is the predominant CO_2 dissociation process, which is the most energy-efficient mechanism, and in this case, the highest asymmetric mode levels V(11)–V(21) contribute for 99.9% to the total vibrational dissociation. This explains why the energy efficiency at 1000 K is much higher than at a higher gas temperature. The energy efficiency of the thermal process is limited because the energy inserted in the plasma is equally distributed over all degrees of freedom of the plasma-chemical system, while only a few of them are important for the CO_2 dissociation. At 1000 K, the energy is selectively used to populate the higher vibrational levels, which are important for the CO_2 dissociation, so this clearly demonstrates that it is important to keep the temperature inside the arc low, in order to achieve the highest energy efficiency. The latter can be realized in practice by using a high frequency GA discharge, in which the arc does not have enough time to be heated to a high value. Indeed, for instance in [86] a higher conversion was observed when the frequency of the GA increased from 15 to 20 kHz.

5.3.2. Effect of the power density

As we already showed in Section 5.2, at a gas temperature of 1200 K, the higher asymmetric mode vibrational levels are not very important in a GA discharge at the power conditions under investigation, and the CO_2 conversion only slightly increases from 6.8% to 8.4% when the power rises from 70 to 100 W. So the question arises whether these higher asymmetric mode vibrational levels are really not important in a GA discharge at this common temperature of 1200 K, and whether or how we could further improve the conversion in this power range. In order to answer these questions, we performed calculations using the same plasma power of 70–100 W, but with a constant arc radius of 0.5 mm for all power values. In this case, the obtained power densities are 3.56×10^4, 4.07×10^4, 4.58×10^4 and 5.09×10^4 W/cm^3, respectively. Thus, in this section, we present the effect of somewhat larger power densities on the CO_2 conversion and on the VDF.

Fig. 14 illustrates that the CO_2 conversion rises significantly from 6.8% to 19.8% in the same power range of 70–100 W. It should be noted that the conversion is limited to a maximum of 20% by the treated gas fraction. The energy efficiency also first increases from 30% to 66% in the power density range of $3.6–4.6 \times 10^4$ W/cm^3, while further increasing the power density to 5.1×10^4 W/cm^3 yields a slight drop in the energy efficiency to 61%. The latter is caused by the fact that the conversion rises to a lower extent than the SEI. However, these results clearly reveal that both the conversion and energy efficiency are greatly improved at these larger power density conditions. In practice, a large power density can be achieved in a micro-scale GA reactor, and it was indeed experimentally demonstrated [57] that such a micro-scale GA reactor results in a higher conversion. On the other hand, it should also be realized that the amount of gas that can be treated in a micro-scale GA reactor is more limited. However, we believe that

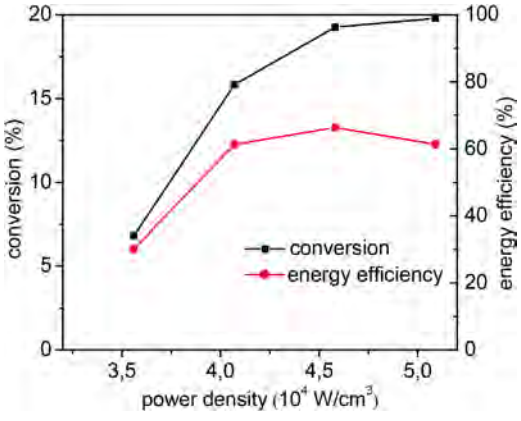

Fig. 14. Calculated CO_2 conversion and energy efficiency as a function of power density, at a gas flow rate of 6.5 L/min and a shortest interelectrode gap of 2.5 mm.

the latter could be compensated in practice by placing a number of GA reactors in parallel, as has been demonstrated already for other gas conversion applications (i.e., ozone production) by placing a large number of DBD reactors in parallel [87].

As mentioned above, it was discussed in Section 5.2 that the role of the higher asymmetric mode vibrational levels of CO_2 was negligible, and the symmetric mode and lower asymmetric mode vibrational levels are mainly important for the CO_2 splitting process at a gas temperature of 1200 K inside the arc. In Fig. 15, we plot the normalized VDF of the asymmetric mode of CO_2, at a time of 8 ms, for the four different power density values investigated. It is obvious that the population of the higher asymmetric mode vibrational levels drastically increases when the power density rises from 3.6×10^4 W/cm^3 to 4.1×10^4 W/cm^3, and this explains the significant rise in the CO_2 conversion, since these higher vibrational levels become increasingly important for the CO_2 dissociation, which is essential for energy-efficient CO_2 splitting. Indeed, at the power density of 4.1×10^4 W/cm^3, the highest asymmetric mode vibrational levels V(11)-V(21) contribute for 99.3% to the dissociation of the vibrationally excited states of CO_2 upon collision with any neutral species (M) and the O atoms, and their contribution increases to 99.7% at the power densities of 4.6×10^4 and 5.1×10^4 W/cm^3. However, at the power density of 4.1×10^4 W/cm^3, the dissociation of vibrationally excited states of CO_2 upon collision with any neutral species (M) or the O atoms is not very important as CO_2 dissociation mechanism, while it is more important at the higher power densities. This explains why the CO_2 conversion and energy efficiency rise upon increasing power density. At the power density of 3.6×10^4 W/cm^3, the contribution of the highest asymmetric vibrational levels V(11)-V(21) to the dissociation of vibrationally excited states of CO_2 upon collision with M or O atoms is still very high, i.e., about 97%, but again this process is not so important for the overall CO_2 conversion. Indeed, at this power density, the electron impact dissociation of vibrationally excited states of CO_2 is the most important splitting mechanism, in which the symmetric and lower asymmetric vibrational levels play the most important role, and the higher asymmetric vibrational levels have almost no contribution to the dissociation of CO_2. This analysis clearly indicates that the importance of the higher asymmetric mode vibrational levels for the CO_2 dissociation strikingly depends on the GA discharges conditions.

The most important processes responsible for the CO_2 conversion are plotted in Fig. 16, as a function of the power density. At the low plasma power density, similar to the results

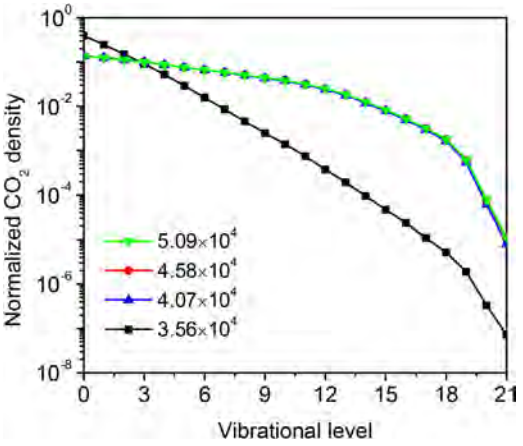

Fig. 15. Normalized vibrational distribution functions of the asymmetric mode of CO_2 in the GA discharge at t = 8 ms, for different power density values, at a gas flow rate of 6.5 L/min and a shortest interelectrode gap of 2.5 mm.

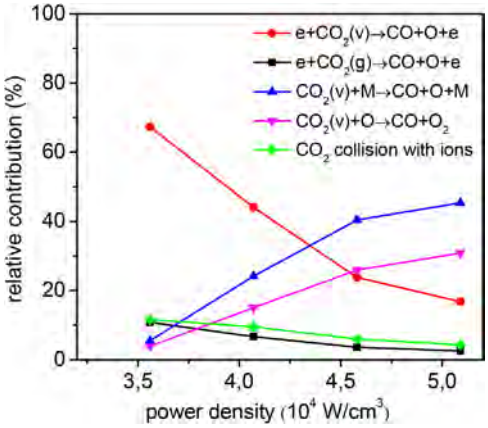

Fig. 16. Relative contributions of the most important loss processes of CO_2, integrated over the entire gas residence time, as a function of power density.

shown in Section 5.2, the main splitting reaction is electron impact dissociation of vibrationally excited states of CO_2 into CO and O. However, with increasing plasma power density, the dissociation of vibrationally excited states upon collision with any neutral species (M), and with O atoms, begin to play the most important role in the CO_2 dissociation, contributing for about 45% and 31%, respectively, at the power density of 5.1×10^4 W/cm^3, while electron impact dissociation of the vibrationally excited states now only contributes for about 17% to the overall CO_2 conversion. As dissociation of the vibrationally excited CO_2 levels upon collision with any neutral species (M) or with the O atoms is a more energy-efficient process than electron impact dissociation of the vibrationally excited levels, this explains the better energy efficiency at the higher power densities investigated.

As far as the CO_2 formation processes are concerned, the recombination reaction of CO with O atoms and a third body (M) is the predominant production mechanisms of CO_2 at all plasma power densities investigated, with a relative contributions of about 85%, hence the same as obtained in Section 5.2. Therefore, to increase the CO_2 conversion and energy efficiency, we believe that this recombination reaction should be reduced, as will be discussed in the next section.

5.3.3. *Effect of the backward reaction between CO and O atoms*

To illustrate that the recombination reaction of CO with O is indeed limiting the conversion and energy efficiency, we have set the reaction rate coefficient of this reaction equal to zero, to investigate its effect on the conversion and energy efficiency. In this case, no reverse reaction $CO + O + M \rightarrow CO_2 + M$ will occur. This is of course an artificial correction in the model, but it allows us to evaluate what would be the effect of preventing the back-reaction, for instance by removing the O atoms from the mixture (see below).

Fig. 17 shows a comparison between the overall CO_2 conversion calculated with the original and the modified reaction set, obtained at a plasma power of 70 W and a gas flow rate of 6.5 L/min, assuming a gas temperature inside the arc of 1200 K. It is clear that the conversion more than doubles, from 6.8% to 19.8% (i.e., nearly the maximum possible, because of the limited gas fraction treated), while the energy efficiency rises from 31% up to 88%. A similar behavior was also observed in experiments [56], where the maximum CO_2 conversion was 12.3% in pure CO_2, while it increased to 34.5% when methane was injected as additive. We believe that the oxygen was indeed preferably consumed in the reforming reaction of CH_4, so the injection of CH_4 limits the recombination of CO and O into CO_2, thereby increasing the CO_2 conversion.

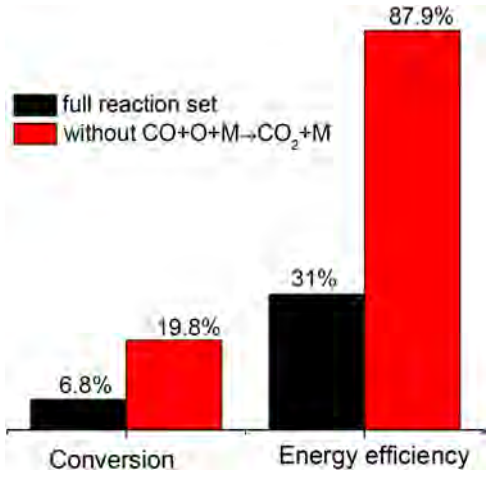

Fig. 17. Effect of removing the recombination reaction ($CO + O + M \rightarrow CO_2 + M$) from the model, on the calculated CO_2 conversion and energy efficiency, for a plasma power of 70 W, a gas flow rate of 6.5 L/min and a shortest interelectrode gap of 2.5 mm.

As mentioned above, in order to reduce the backward reaction between CO and O atoms, we believe it would be necessary to remove the O atoms from the mixture, so that there is not enough reactant available for this back-reaction from CO into CO_2. It should be noted that in our modeling study for a microwave discharge [68], we pointed out that the O atoms should preferentially react with CO_2 (to form CO and O_2) in order to improve the energy efficiency, before they would recombine with another O atom or with an O_2 molecule, into an O_2 or O_3 molecule, respectively, while here we suggest that it is better to remove the O atoms (e.g., by letting them react with O_2, into the formation of O_3), to avoid their recombination with CO into CO_2. The reason for this difference is that in the microwave discharge studied in [68], the collision of CO_2 with O atoms is indeed crucial to further improve the CO_2 conversion, while in the GA discharge investigated here, electron impact dissociation plays a key role in the CO_2 conversion, and the relative contribution of CO_2 collisions with O atoms to the overall CO_2 conversion is quite low. Thus, if the role of the O atoms in the recombination process is more important than its role in the dissociation process of CO_2, it is important to be able to remove the O atoms, as the latter will further improve the conversion of CO_2, while not having a negative effect on the conversion.

In order to remove the O atoms from the mixture in practice, with the aim to achieve a higher conversion, we believe that possible scavengers, catalyst interactions or membrane technology might be an option. The main idea to eliminate the O atoms is to find an interaction which makes the O atoms no longer available as a reactant; hence, this interaction has to be significantly faster than the reaction between CO and O. One possible scavenger for the O atoms could be H atoms. Indeed, it was demonstrated in [88] that the O atoms can be chemically trapped during the plasma splitting of CO_2 by the addition of H_2 or CH_4, forming H_2O. We believe that this is also the reason why in the experiments of ref. [56], the maximum CO_2 conversion increased from 12.3% to 34.5% upon addition of methane, as mentioned above, because the O atoms are probably preferentially consumed in the reforming reaction of CH_4, so the addition of CH_4 limits the recombination of CO and O into CO_2, thereby increasing the CO_2 conversion. With respect to the catalyst interactions, a more advanced catalytic process would be an alternative form of chemical looping, in which the O or O_2 is captured in the plasma set-up and then used as an oxidizing agent in a second set-up [89,90]. Finally, by means of membrane separation technology, the O atoms (or O_2 molecules) could possibly be transported away from the reaction mixture. The combination of a solid oxide electrolyser cell with a plasma set-up could also be an option. In [91] a maximum CO_2 conversion of 40% was obtained for a DBD plasma reactor, but this conversion was increased to about 80% by removing O_2 from the plasma in a hybrid reactor with a solid oxide electrolyser cell. It should, however, be realized that these options for catalysts or membrane technology have only been successfully applied up to now to separate O_2 from the plasma. In order to trap the O atoms, we believe that adding possible scavengers, as mentioned above, could be a good choice. Nevertheless, it should be mentioned that these ways of removing O atoms from the mixture are only suggestions, and they were not experimentally verified yet for our setup, although we indeed have indications that the chemical trapping should work, as demonstrated in the cited references above.

5.4. How do the conversion and energy efficiency of a GA discharge compare with other types of plasma reactors?

Our experimental and calculation results illustrate that the CO_2 conversion is in the range of 6–10%, while the energy efficiency reaches about 40%. Moreover, our calculations predict that by reducing the gas temperature inside the arc, or by enhancing the power density (e.g., by applying a micro-scale GA reactor), or by reducing the main reverse reaction, the conversion and energy efficiency can reach values up to nearly 20% (i.e., the maximum possible for a treated gas fraction of 20%) and nearly 100%, respectively, although it should be realized that these model predictions are of course upper limits. Nevertheless, they show how the conversion and energy efficiency could be further improved, which is very useful to guide further experimental optimization work. In Fig. 18 we compare our results with data obtained from literature for CO_2 splitting, in a GA discharge, as well as in other types of plasma reactors, such as a DBD and a microwave (MW) plasma, a ns-pulse or spark discharge.

As Fig. 18 shows the optimim values for conversion and energy efficiency available in the literature, we also only plot our best obtained results, and we also added our model predictions, based on the suggested improvements discussed in Section 5.3 (see below). In order to realize a fair assessment for industrial applicability, we only compare with results from literature obtained at atmospheric pressure, although it should be mentioned that in a microwave discharge, a higher energy efficiency of 60% [92] and even up to 80–90% [10] was obtained at a reduced pressure and supersonic gas flow.

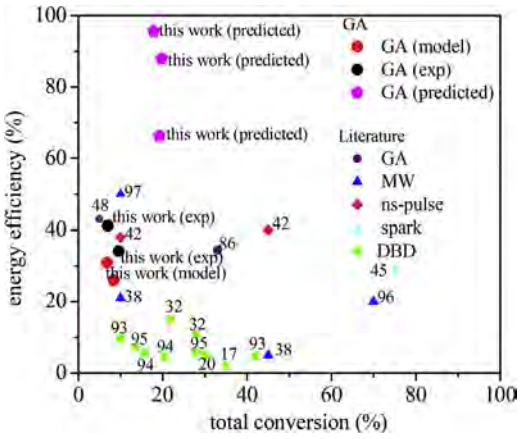

Fig. 18. Comparison of our (experimental and calculated) values of energy efficiency vs. conversion, with experimental data for various discharge types collected from literature, as indicated in the legend. The numbers associated with the data points correspond to the references in this paper.

It is clear from Fig. 18 that a DBD [17,20,32,93–95] has a reasonable conversion but a quite low energy efficiency. Microwave discharges also show limited performance up to now for conversion and energy efficiency, at least when they operate at atmospheric pressure conditions. An energy efficiency of only about 20% was reported at normal flow conditions [96], although at reverse vortex flow conditions, an energy efficiency up to 50% was obtained [97]. In general, GA plasmas exhibit a better performance in terms of energy efficiency, with respect to DBDs and microwave discharges, and similar to ns-pulse and spark discharges. In [86], a maximum CO_2 conversion of 33% was reported, but this was upon addition of CH_4, and is attributed to the fact that the O atoms have a higher possibility to react with H atoms originating from CH_4, instead of contributing to the backward reaction, as pointed out in Section 5.3.3. Moreover, the authors used a higher frequency of 20 kHz, which will result in less gas heating, and thus in a higher conversion, as discussed in Section 5.3.1.

In spite of the reasonable results obtained already in a GA, the conversion should still be further improved, while maintaining the high energy efficiency. We believe that this could be realized either by reducing the gas temperature inside the arc, applying a micro-scale GA with higher power density, or by removing the reverse reactions, as presented in previous sections, because in these cases, the calculated conversion was found to increase up to nearly 20%, with energy efficiencies reaching up to nearly 100%. These model predictions are also indicated in Fig. 18. However, the small treated gas fraction (i.e., about 20%) is still the major limiting factor for the conversion, so we believe that a better design of the reactor is needed to improve the treated gas volume. One way to do so is by applying a reverse vortex flow GA reactor [48,98]. Another way, which can be applied in a classical GA reactor, could be to exploit the so-called back-breakdown phenomenon, which results in a larger gas flow velocity compared to the arc velocity [66,99–101], so that more gas can be treated by the arc. In summary, we believe that a GA plasma still has room for improvement by optimizing the gas fraction to be treated, and that it will have great potential for gas processing applications.

6. Conclusions

CO_2 splitting by means of plasma technology is gaining increasing interest, and a gliding arc (GA) plasma is one of the most promising plasma setups for this purpose. However, the underlying mechanisms and chemical pathways are still far from understood. Therefore, in this work we try to obtain a better understanding of the underlying chemical mechanisms of CO_2 splitting in a GA discharge, by means of a 0D chemical kinetics model, using assumptions based on our previous 2D and 3D models.

A comparison is made between the calculated and measured CO_2 conversion and energy efficiency for various conditions, and the conversion was typically in the order of 6–10%, while the energy efficiency was around 20–40%. These are reasonable values when compared to other plasma technologies, but they are also still subject to improvement. A very good agreement was reached between the calculated and experimental data, indicating that the model can be used to identify the important species and reactions playing a role in the CO_2 splitting, i.e., the main production and loss pathways of CO_2. This allows us to gain sufficient insight into the entire process, and to identify the limiting factors for CO_2 conversion, and thus to propose solutions for improving the CO_2 conversion based on the chemical reaction pathway analysis.

Our study clearly reveals that in the experimental plasma power range of 70–100 W, electron impact dissociation of CO_2 molecules in vibrational levels (i.e., $CO_2(v) + e \rightarrow CO + O + e$) is the main loss pathway of CO_2 at a gas temperature inside the arc of 1200 K. Because of the crucial role of the vibrationally excited states of CO_2 for energy-efficient dissociation, we investigated the vibrational distribution functions (VDFs) of the asymmetric mode of CO_2 at different values of the plasma power. The populations of the vibrational levels slightly rise with increasing plasma power, which explains the rise in the CO_2 conversion with plasma power. However, at the conditions investigated, mainly the lower asymmetric mode and symmetric mode vibrational levels of CO_2 are important for CO_2 splitting, which limits the energy efficiency. Moreover, for all plasma powers investigated, the three-body recombination between CO and O atoms (i.e., $CO + O + M \rightarrow CO_2 + M$) is the main production process for CO_2, and this limits the conversion. Thus, in order to further improve the CO_2 conversion, the reversion reaction should be inhibited or at least reduced.

As we were able to identify the limiting factors that prevent a higher and more energy-efficient CO_2 conversion, we can propose solutions on how this process can be further improved. First, our model predicts that when the gas temperature inside the arc could be reduced to 1000 K, the conversion and energy efficiency would increase up to 18% and 96%, respectively, because (i) the reverse reaction between CO and O atoms is significantly reduced, as the O atoms are more efficiently used for other reactions (i.e., O_3 formation) at low temperature, and (ii) the higher vibrationally excited levels become much more important (see below). On the other hand, increasing the gas temperature up to 3000 K also yields a significant rise in the CO_2 conversion up to 16.5%, but the energy efficiency is only about 29%. In this case, the plasma is only a provider of the required high temperature to speed up the chemical reactions, but the energy inserted in the plasma is equally distributed over the various degrees of freedom, and the advantages of non-equilibrium vibrational excitation of CO_2 disappear. Indeed, by investigating the VDFs of the asymmetric mode of CO_2 at various gas temperatures, we found that the populations of the higher asymmetric mode vibrational levels are very low at a gas temperature of 1200–3000 K, so they are not important for the dissociation of CO_2. However, at a gas temperature of 1000 K, the densities of the higher asymmetric mode vibrational levels are very large, pointing towards a clear non-equilibrium situation, and leading to a higher CO_2 conversion and energy efficiency. Reducing the temperature inside the arc might be realized in practice by means of a high frequency GA discharge, so that the arc has not enough time to heat up.

Second, by increasing the power density, both the conversion and energy efficiency show a significant improvement, reaching up to 19% and 66% respectively, at a power density of 4.6×10^4 W/cm^3. These calculations were performed in the same experimental power range of 70–100 W, but the power density increases from 3.6×10^4 to 5.1×10^4 W/cm^3 by using a constant arc column radius of 0.5 mm. At a larger power density, the dissociation of vibrationally excited states of CO_2 upon collisions with any neutral species (M) or with O atoms become the most important CO_2 splitting mechanisms. Moreover, the higher asymmetric mode vibrational states play an important role in the splitting process, resulting in a higher conversion and energy efficiency. In practice, we believe that a higher power density could be achieved by applying a micro-scale GA reactor, as also demonstrated in literature [57].

Third, we demonstrate by our model that if the O atoms, formed by the CO_2 splitting, could be removed from the system, e.g., by chemical trapping with H atoms, the most important reverse reaction, i.e., the three-body recombination of CO with O atoms forming again CO_2, could be blocked, and consequently, the CO_2 conversion and energy efficiency can increase by again more than a factor two.

Finally, we believe that the conversion in the GA discharge could be further enhanced by increasing the fraction of treated gas

in the arc. Indeed, the improvements proposed above can achieve a theoretical conversion of nearly 20%, along with a theoretical energy efficiency of 100%, but the conversion cannot exceed 20%, because this corresponds to the fraction of gas that passes through the arc, as assumed in the model, while the other gas fraction flows through the reactor without passing through the arc. Increasing the gas fraction treated by the arc can be realized experimentally if the gas flow velocity is larger than the arc velocity, which can be the result of the so-called back-breakdown phenomenon, which reduces the arc velocity [99–101]. In experiments, some operating parameters can be adjusted to control the occurrence of the back-breakdown process, such as the gas flow rate, the current and the reactor structure. Other possible solutions could be modifications to the reactor design, allowing more gas to pass through the arc, like in a reverse vortex flow GA discharge [48,98].

By comparing our results with other commonly used plasma reactors for CO_2 conversion, we can conclude that the energy efficiency of CO_2 splitting in a GA discharge is indeed very promising, and better than in other plasma types at atmospheric pressure. However, the corresponding conversion should be further improved in order to make the GA plasma technique more competitive with other technologies. We believe that a better understanding of the CO_2 splitting mechanisms in a GA discharge, as obtained in this study, is very valuable, as it allow us to propose solutions on how to improve the conversion, which can guide further experimental optimizations.

Acknowledgments

We acknowledge financial support from the IAP/7 (Inter-university Attraction Pole) program 'PSI-Physical Chemistry of Plasma-Surface Interactions' by the Belgian Federal Office for Science Policy (BELSPO) and the Fund for Scientific Research Flanders (FWO; Grant no. G.0383.16N). The calculations were carried out using the Turing HPC infrastructure at the CalcUA core facility of the Universiteit Antwerpen (UAntwerpen), a division of the Flemish Supercomputer Center VSC, funded by the Hercules Foundation, the Flemish Government (department EWI) and the UAntwerpen. This work is also supported by National Natural Science Foundation of China (grant nos. 11275021, 11575019). S R Sun thanks the financial support from the China Scholarship Council (CSC).

References

[1] J.J. Shah, H.B. Singh, Environ. Sci. Technol. 22 (12) (1988) 1381–1388.
[2] J. Qiao, Y. Liu, F. Hong, J. Zhang, Chem. Soc. Rev. 43 (2014) 631–675.
[3] M. Aresta, A. Dibenedetto, A. Angelini, Chem. Rev. 114 (2014) 1709–1742.
[4] Eric E. Benson, Clifford P. Kubiak, Aaron J. Sathrum, Jonathan M. Smieja, Chem. Soc. Rev. 38 (2009) 89–99.
[5] J. Shi, Y. Jiang, Z. Jiang, X. Wang, X. Wang, S. Zhang, P. Han, C. Yang, Chem. Soc. Rev. 44 (2015) 5981–6000.
[6] S.D. Ebbesen, S.H. Jensen, A. Hauch, M.B. Mogensen, Chem. Rev. 114 (2014) 10697–10734.
[7] W. Wang, S. Wang, X. Ma, J. Gong, Chem. Soc. Rev. 40 (2011) 3703–3727.
[8] A. Goeppert, M. Czaun, J.P. Jones, G.K.S. Prakash, G.A. Olah, Chem. Soc. Rev. 43 (2014) 7995–8048.
[9] Y. Ma, X. Wang, Y. Jia, X. Chen, H. Han, C. Li, Chem. Rev. 114 (2014) 9987–10043.
[10] A. Fridman, Plasma Chemistry, Cambridge University Press, Cambridge, 2008.
[11] I.A. Semiokhin, Y.P. Andreev, G.M. Panchenkov, Russ. J. Phys. Chem. 38 (8) (1964) 1126.
[12] A.N. Maltsev, E.N. Eremin, L.V. Ivanter, Russ. J. Phys. Chem. 41 (1967) 633.
[13] Y.P. Andreev, I.A. Semiokhin, Y.M. Voronkov, V.A. Sirotkina, V.A. Kaigorodov, Russ. J. Phys. Chem. 45 (1971) 1587.
[14] V.D. Rusanov, A.A. Fridman, G.V. Sholin, Sov. Phys.—Usp. 24 (6) (1981) 447–474.
[15] R.I. Asisov, A.A. Fridman, V.K. Givotov, E.G. Krasheninnikov, B.I. Petrushev, B.V. Potapkin, V.D. Rusanov, M.F. Krotov, I.V. Kurchatov, Carbon dioxide dissociation in non-equilibrium plasma, 5th Int Symp. on Plasma Chemistry, Edinburgh, UK, 1981, pp. 774.
[16] R.I. Azizov, A.K. Vakar, V.K. Zhivotov, M.F. Krotov, O.A. Zinov'ev, B.V. Potapkin, V.D. Rusanov, A.A. Rusanov, A.A. Fridman, Sov. Phys. Dokl. 28 (7) (1983) 567–569.
[17] R. Aerts, W. Somers, A. Bogaerts, ChemSusChem 8 (2015) 702–716.
[18] R. Snoeckx, R. Aerts, X. Tu, A. Bogaerts, J. Phys. Chem. C 117 (2013) 4957–4970.
[19] R. Snoeckx, Y.X. Zeng, X. Tu, A. Bogaerts, RSC Adv. 5 (2015) 29799–29808.
[20] X. Tu, J.C. Whitehead, Appl. Catal. B: Environ. 125 (2012) 439–448.
[21] M. Scapinello, L.M. Martini, P. Tosi, Plasma Proc. Polym. 11 (7) (2014) 624–628.
[22] R. Aerts, R. Snoeckx, A. Bogaerts, Plasma Process. Polym. 11 (10) (2014) 985–992.
[23] C. De Bie, J. van Dijk, A. Bogaerts, J. Phys. Chem. C 119 (2015) 22331–22350.
[24] N.R. Pinhao, A. Janeco, J.B. Branco, Plasma Chem. Plasma Proc. 31 (2011) 427–439.
[25] M. Ramakers, I. Michielsen, R. Aerts, V. Meynen, A. Bogaerts, Plasma Process. Polym. 12 (2015) 755–763.
[26] Q. Wang, Y. Cheng, Y. Jin, Catal. Today 148 (2009) 275–282.
[27] A.J. Zhang, A.M. Zhu, J. Guo, Y. Xu, C. Shi, Chem. Eng. J. 156 (2010) 601–606.
[28] T. Nozaki, K. Okazaki, Catal. Today 211 (2013) 29–38.
[29] A. Ozkan, T. Dufour, G. Arnoult, P. De Keyzer, A. Bogaerts, F. Reniers, J. CO_2 Util. 9 (2015) 74–81.
[30] S. Paulussen, B. Verheyde, X. Tu, C. De Bie, T. Martens, D. Petrovic, A. Bogaerts, B. Sels, Plasma Sour. Sci. Technol. 19 (2010) 034015.
[31] B. Eliasson, U. Kogelschatz, B. Xue, L.M. Zhou, Ind. Eng. Chem. Res. 37 (1998) 3350–3357.
[32] A. Ozkan, T. Dufour, T. Silva, N. Britun, R. Snyders, A. Bogaerts, F. Reniers, Plasma Sour. Sci. Technol. 25 (2016) 025013.
[33] A. Ozkan, T. Dufour, A. Bogaerts, F. Reniers, Plasma Sour. Sci. Technol. 25 (2016) 045016.
[34] A. Ozkan, T. Dufour, T. Silva, N. Britun, R. Snyders, F. Reniers, A. Bogaerts, Plasma Sour. Sci. Technol. 25 (2016) 055005.
[35] N. Britun, T. Godfroid, R. Snyders, Plasma Sour. Sci. Technol. 21 (2012) 035007.
[36] T. Silva, N. Britun, T. Godfroid, R. Snyders, Plasma Sour. Sci. Technol. 23 (2014) 025009.
[37] A. Vesel, M. Mozetic, A. Drenik, M. Balat-Pichelin, Chem. Phys. 382 (2011) 127–131.
[38] L.F. Spencer, A.D. Gallimore, Plasma Sour. Sci. Technol 22 (2013) 015019.
[39] S. Heijkers, R. Snoeckx, T. Kozak, T. Silva, T. Godfroid, N. Britun, R. Snyders, A. Bogaerts, J. Phys. Chem. C 119 (23) (2015) 12815–12828.
[40] G. Chen, T. Silva, V. Georgieva, T. Godfroid, N. Britun, R. Snyders, M.P. Delplancke-Ogletree, Int. J. Hydrog. Energy 40 (20) (2015) 3789–3796.
[41] G. Chen, V. Georgieva, T. Godfroid, R. Snyders, M.P. Delplancke-Ogletree, Appl. Catal. B: Environ. 190 (2016) 115–124.
[42] M. Scapinello, L.M. Martini, G. Dilecce, P. Tosi, J. Phys. D: Appl. Phys. 49 (2016) 075602.
[43] X.S. Li, B. Zhu, C. Shi, Y. Xu, A.M. Zhu, AIChE J. 57 (2011) 2854–2860.
[44] B. Zhu, X.S. Li, C. Shi, J.L. Liu, T.L. Zhao, A.M. Zhu, Int. J. Hydrog. Energy 37 (2012) 4945–4954.
[45] B. Zhu, X.S. Li, J.L. Liu, X. Zhu, A.M. Zhu, Chem. Eng. J. 264 (2015) 445–452.
[46] V. Shapoval, E. Marotta, C. Ceretta, N. Konjevic, M. Ivkovic, M. Schiorlin, C. Paradisi, Plasma Process. Polym. 11 (2014) 787–797.
[47] V. Shapoval, E. Marotta, Plasma Process. Polym. 12 (2015) 808–816.
[48] T. Nunnally, K. Gutsol, A. Rabinovich, A. Fridman, A. Gutsol, A. Kemoun, J. Phys. D Appl. Phys. 44 (27) (2011) 274009.
[49] A. Indarto, D.R. Yang, J.W. Choi, H. Lee, H.K. Song, J. Hazard. Mater. 146 (2007) 309–315.
[50] A. Indarto, J.W. Choi, H. Lee, H.K. Song, Environ. Eng. Sci. 23 (6) (2006) 1033–1043.
[51] Z. Bo, J. Yan, X. Li, Y. Chi, K. Cen, Int. J. Hydrog. Energy 33 (20) (2008) 5545–5553.
[52] Y.C. Yang, B.J. Lee, Y.N. Chun, Energy 34 (2) (2009) 172–177.
[53] X. Tu, J.C. Whitehead, Int. J. Hydrog. Energy 39 (18) (2014) 9658–9669.
[54] N. Rueangjitt, T. Sreethawong, S. Chavadej, Plasma Chem. Plasma Process. 28 (2008) 49–67.
[55] N. Rueangjitt, C. Akarawitoo, T. Sreethawong, S. Chavadej, Plasma Chem. Plasma Process. 27 (2007) 559–576.
[56] S.C. Kim, M.S. Lim, Y.N. Chun, Plasma Chem. Plasma Process. 34 (2014) 125–143.
[57] N. Rueangjitt, T. Sreethawong, S. Chavadej, H. Sekiguchi, Chem. Eng. J. 155 (3) (2009) 874–880.
[58] A. Wu, J. Yan, H. Zhang, M. Zhang, C. Du, X. Li, Int. J. Hydrog. Energy 39 (2014) 17656–17670.
[59] X. Li, H. Zhang, S. Yan, J. Yan, C. Du, IEEE Trans. Plasma Sci. 41 (1) (2013) 126–132.
[60] K. Li, J.L. Liu, X.S. Li, X. Zhu, A.M. Zhu, Chem. Eng. J. 288 (2016) 671–679.
[61] A. Fridman, S. Nester, L.A. Kennedy, A. Saveliev, O. Mutaf-Yardimci, Prog. Energy Combust. Sci. 25 (1999) 211–231.
[62] O. Mutaf-Yardimci, A.V. Saveliev, A.A. Fridman, L.A. Kennedy, J. Appl. Phys. 87 (4) (2000) 1632–1641.
[63] I.V. Kuznetsova, N.Y. Kalashnikov, A.F. Gutsol, A.A. Fridman, L.A. Kennedy, J. Appl. Phys. 92 (8) (2002) 4231–4237.
[64] A. Czernichowski, Pure Appl. Chem. 66 (6) (1994) 1301–1310.
[65] St. Kolev, A. Bogaerts, Plasma Sour. Sci. Technol. 24 (2015) 015025.
[66] S. Sun, St. Kolev, H.X. Wang, A. Bogaerts, Plasma Sour. Sci. Technol. 26 (2017) 015003.
[67] T. Kozak, A. Bogaerts, Plasma Sour. Sci. Technol. 23 (2014) 045004.
[68] T. Kozak, A. Bogaerts, Plasma Sour. Sci. Technol. 24 (2015) 015024.

[69] X. Tu, H.J. Gallon, J.C. Whitehead, Electrical and optical diagnostics of atmospheric pressure argon gliding arc plasma jet, 30th Int Conf. on Phenomena in Ionized Gases, Belfast, UK, 28 August–2 September 2011, 2011, pp. C10.
[70] X. Tu, H.J. Gallon, J.C. Whitehead, IEEE Trans. Plasma Sci. 39 (2011) 2900–2901.
[71] S. Pancheshnyi, B. Eismann, G.J.M. Hagelaar, L.C. Pitchford, Computer Code ZDPlasKin, University of Toulouse, LAPLACE, CNRS-UPS-INP, Toulouse, France, 2008. http://www.zdplaskin.laplace.univ-tlse.fr.
[72] A. Berthelot, A. Bogaerts, Plasma Sour. Sci. Technol. 25 (2016) 045022.
[73] P. Koelman, S. Heijkers, S. Tadayon Mousavi, W. Graef, D. Mihailova, T. Kozák, A. Bogaerts, J. van Dijk, A comprehensive chemical model for the splitting of CO_2 in non-equilibrium plasmas, Plasma Process Polym. (2016) in press).
[74] Phelps Database, www.lxcat.net (retrieved on 1 December 2015).
[75] G.J.M. Hagelaar, L.C. Pitchford, Plasma Sour. Sci. Technol. 14 (2005) 722–733.
[76] A. Bogaerts, W. Wang, A. Berthelot, V. Guerra, Plasma Sour. Sci. Technol. 25 (2016) 055016.
[77] N. Pinhao, A. Moura, J.B. Branco, J. Neves, Int. J. Hydrog. Energy 14 (22) (2016) 9245–9255.
[78] F. Richard, J.M. Cormier, S. Pellerin, J. Chapelle, J. Appl. Phys. 79 (1996) 2245.
[79] S. Pellerin, F. Richard, J. Chapelle, J.M. Cormier, K. Musiol, J. Phys. D Appl. Phys. 33 (2000) 2407–2419.
[80] A. Czernichowski, H. Nassar, A. Ranaivosoloarimanana, Acta Phys. Pol., A 89 (1996) 595–603.
[81] A. Czernichowski, Oil & gas science and technology −Rev, IFP 56 (2) (2001) 181–198.
[82] S.P. Gangoli, Experimental and Modeling Study of Warm Plasmas and Their Applications. PhD Thesis, Drexel University, 2007.
[83] I. Rusu, J.M. Cormier, Chem. Eng. J. 91 (1) (2003) 23–31.
[84] F. Ouni, A. Khacef, J.M. Cormier, Chem. Eng. Technol. 29 (5) (2006) 604–609.
[85] J.M. Cormier, I. Rusu, M. Dudemaine, D. Sibiescu, Proc. 4th Int Conf. Optimization of Electrical and Electronic Equipments OPTIM'1, Brasov, 2002.
[86] A. Indarto, J.W. Choi, H. Lee, H.K. Song, Energy 31 (2006) 2986–2995.
[87] U. Kogelschatz, Plasma Chem. Plasma Process. 23 (1) (2003) 1–46.
[88] R. Aerts, R. Snoeckx, A. Bogaerts, Plasma Process. Polym. 11 (2014) 985–992.
[89] R. Snoeckx, S. Heijkers, K. Van Wesenbeeck, S. Lenaerts, A. Bogaerts, Energy Environ. Sci. 9 (2016) 999–1011.
[90] J. Adanez, A. Abad, F. Garcia-Labiano, P. Gayan, L.F. de Diego, Prog. Energy Combust. Sci. 38 (2012) 215–282.
[91] Y. Tagawa, S. Mori, M. Suzuki, I. Yamanaka, T. Obara, J. Ryu, Y. Kato, Kagaku Kogaku Ronbunshu 37 (2) (2011) 114–119.
[92] A.P.H. Goede, W.A. Bongers, M.G. Graswinckel, R.M.C. van de Sanden, L. Martina, K. Jochen, A. Schulz, W. Mathias, 3rd Eur. Energy Conf. Budapest (2013).
[93] K. Van Laer, A. Bogaerts, Energy Technol. 3 (2015) 1038–1044.
[94] Q. Yu, M. Kong, T. Liu, J. Fei, X. Zheng, Plasma Chem. Plasma Process. 32 (2012) 153–163.
[95] D. Mei, X. Zhu, Y. He, J.D. Yan, X. Tu, Plasma Sour. Sci. Technol. 24 (2015) 015011.
[96] J.Q. Zhang, J.S. Zhang, Y.J. Yang, Q. Liu, Energy Fuels 17 (1) (2003) 54–59.
[97] M. Leins, S. Gaiser, J. Kopecki, W.A. Bongers, A. Goede, M.F. Graswinckel, A. Schulz, M. Walker, M.C.M. van de Sanden, T. Hirth, 22nd International Symposium on Plasma Chemistry, P-II-8-18, Antwerp Belgium, 2015.
[98] G. Trenchev, St. Kolev, A. Bogaerts, Plasma Sour. Sci. Technol. 25 (2016) 035014.
[99] S. Pellerin, O. Martinie, J.M. Cormier, J. Chapelle, P. Lefaucheux, High Temp. Mater. Process. 3 (2) (1999) 167–180.
[100] J. Zhu, Z. Sun, Z. Li, A. Ehn, M. Alden, M. Salewski, F. Leipold, Y. Kusano, J. Phys. D: Appl. Phys. 47 (29) (2014) 295203.
[101] F. Mitsugi, J. Furukawa, T. Ohshima, H. Kawasaki, T. Kawasaki, S. Aoqui, H.D. Stryczewska, Eur. Phys. J.: Appl. Phys. 61 (2) (2013) 24308.